https://doi.org/10.5194/egusphere-2026-5074
Preprint. Discussion started: 26 August 2026

Black carbon mixing-state heterogeneity influences absorption enhancement: Results from a field study across three seasons

Yifan Yang[1], Thomas Müller[1], Baseerat Romshoo[1], Jens Voigtländer[1], Mira L. Pöhlker[1,2]

[1]Department of Atmospheric Microphysics, Leibniz Institute for Tropospheric Research, Leipzig, 04318, Germany
[2]Faculty of Physics and Earth Sciences, Leipzig Institute for Meteorology, Leipzig University, 04103, Leipzig, Germany

Correspondence to: Yifan Yang (yang@tropos.de)

Abstract: Black carbon (BC) is the major light-absorbing aerosol and an important contributor to radiative forcing. Atmospheric aging often coats BC with non-absorbing material, enhancing its mass absorption cross-section (MAC). However, this absorption enhancement depends not only on the bulk amount of coating material but also on how the coatings are distributed across individual BC particles. Here, we represent BC mixing-state heterogeneity using particle-resolved two-dimensional mixing-state distributions. This representation provides a more complete explanation of MAC variability than a single bulk mixing-state parameter. During summer, mixing-state heterogeneity changed little, and MAC remained nearly constant despite a substantial increase in the bulk coating-to-core mass ratio. By contrast, larger changes in mixing-state heterogeneity observed during autumn and winter coincided with MAC increases of up to 35% and 30%, respectively. MAC was most sensitive when initially homogeneous BC populations became more heterogeneous, whereas further changes within already heterogeneous populations produced comparatively small responses. A higher fraction of large-core BC particles (>300 nm), associated with biomass and coal combustion, further reduced MAC because of their lower absorbing efficiency. Mie calculations further showed that MAC differed by ~24 % on average under homogeneous and heterogeneous mixing-state assumptions. Our results highlight the importance of explicitly representing BC mixing-state heterogeneity for a better understanding in aerosol optical property variations and improving their simulation in models, thereby reducing uncertainties in estimates of BC radiative forcing.

1. Introduction

Black carbon (BC), also known as soot, is the primary absorbing component in atmospheric aerosols (Bond and Bergstrom, 2007). BC plays an important role in both the regional and global climate systems. According to the sixth Intergovernmental Panel on Climate Change (IPCC, 2021) report, BC contributed to a global temperature increase of approximately 0.1 °C from 1750 to 2019, with an effective radiative forcing estimated to range from −0.28 to 0.41 Wm^{-2}, indicating substantial uncertainty in its climate impact. Improved characterization of BC's physicochemical properties is key to narrowing the uncertainty in its radiative forcing.

https://doi.org/10.5194/egusphere-2026-5074
Preprint. Discussion started: 26 August 2026

BC is primarily emitted from incomplete combustion, such as biomass burning and fossil fuel combustion (Bond et al., 2013). After emissions, BC particles are coated with non-BC materials through condensation and coagulation during atmospheric aging (Liu et al., 2019). The non-BC coating can enhance the BC absorption efficiency by focusing the incident light onto the BC core, commonly referred to as the 'lensing effect' (Jacobson, 2001; Saleh et al., 2015). Lab experiments have further verified the lensing effect, e.g., Schnaiter (2005) measured that the absorption enhancement (E_{abs}) induced by the lensing effect reached up to 2.1 for BC coated with secondary organic compounds in a chamber study, consistent with Mie theory predictions for concentrically coated spheres. Liu et al. (2017) further demonstrated that significant absorption enhancement occurs when the coating-to-BC mass ratio exceeds 3, highlighting the critical role of coating amount in amplifying the lensing effect.

Field measurements have also confirmed the presence of the lensing effect under ambient conditions(Liu et al., 2015b; Wu et al., 2018; Zanatta et al., 2018; Yuan et al., 2021; Yus-Díez et al., 2022; Wang et al., 2023). Wang et al. (2018) observed that the E_{abs} increased with the fraction of thickly coated BC, and the enhancement reached a steady level for cores larger than 170 nm. Zhang et al. (2018) found that high E_{abs} was associated with aerosol photochemical aging and the formation of highly oxidized secondary organic aerosols (SOA), especially in the summertime. In addition, the formation of secondary nitrate and sulfate has also been shown to contribute to absorption enhancement (Chen et al., 2017; Xie et al., 2019).

However, observational evidence for the lensing effect still remains inconsistent. Cappa et al. (2012) reported a small E_{abs} of 6% on average in California, with weak dependence on photochemical aging. Similar findings have been reported elsewhere, indicating limited correlation between BC absorption and average coating-to-core mass ratio (Liu et al., 2015a; Healy et al., 2015; Cappa et al., 2019). The presence of absorbing materials (e.g., brown carbon) within the coating could reduce the absorption enhancement of BC (Lack and Cappa, 2010; Luo et al., 2018; Feng et al., 2021). Additionally, BC particles with fractal-like morphologies tend to exhibit lower E_{abs} compared to those with compact core-shell structures (Wang et al., 2021; Romshoo et al., 2021; Romshoo et al., 2024). Peng et al. (2016) observed that during the initial aging stage, BC transformed from a fractal to a more spherical morphology with minimal variation in absorption, followed by further compaction that resulted in substantial absorption enhancement.

The average coating thickness or the mass ratio of coating to core of the BC population is commonly used to quantify the bulk mixing state of BC. However, within a given bulk BC population, individual particles can exhibit substantial variability in their mixing states. Transmission electron microscopy (TEM) has revealed significant particle-to-particle variability in coating structure and morphology among BC particles from the same sample. (Adachi et al., 2016; Wang et al., 2017). This particle-by-particle mixing state heterogeneity could contribute to the discrepancies in observed absorption enhancement across different studies. Fierce et al. (2020a) demonstrated that accounting for per-particle composition variability and deviations from the idealized core-shell morphology significantly improves the agreement between predicted and observed absorption enhancement in both laboratory and field studies. Although progress has been made in quantifying BC mixing state heterogeneity, its application in field studies remains limited by measurement constraints. Zhai et al. (2022) reported a bimodal distribution of coating thickness, suggesting an uneven distribution of non-BC material across the particle population and

https://doi.org/10.5194/egusphere-2026-5074
Preprint. Discussion started: 26 August 2026

substantial particle-to-particle mixing state heterogeneity, which reduced the absorption enhancement. Similarly, Zhao et al. (2021) and Zeng et al. (2024) found that less homogeneous BC mixing states, as indicated by a mixing state index reflecting rBC and non-rBC mass fraction distributions, corresponded to weaker absorption enhancement.

In this study, field measurements were conducted to investigate how particle-to-particle variability in BC mixing state affects its light absorption. Mixing-state heterogeneity of BC mixing states was characterized by a Single Particle Soot Photometer (SP2, Droplet Measurement Technology, Longmont, CO, USA), which directly reflects the mixing state of individual particles. Seasonal variations in the relationship between BC mixing state and absorption enhancement were also analysed. The results provide new insights into the role of mixing state in BC absorption enhancement, helping to reduce uncertainties in estimates of BC radiative forcing.

2. Method

2.1 Sampling site

The measurement was conducted at the Melpitz research station (12°56'E, 51°32'N, 86 m a.s.l.) of the Leibniz Institute for Tropospheric Research (TROPOS), a rural site located approximately 50 km northeast of Leipzig, Germany, from August 2021 to February 2022. All the instruments used in the study were set up in the same container and operated through a shared sampling inlet. The inlet system consisted of a PM_{10} Andersen impactor positioned approximately 6 meters above ground level, followed by an automatic aerosol diffusion dryer that maintained the relative humidity in the sampling line below 40% (Tuch et al., 2009). The site is surrounded by flat grasslands, agricultural fields, and woodlands extending over several tens of kilometres. There are no orographic features in the immediate vicinity. Measurements at Melpitz are considered representative of long-range transported air masses and background aerosol conditions in Central Europe (Spindler et al., 2012; Spindler et al., 2013). The station is part of several observation networks, such as ACTRIS (Aerosols, Clouds, and Trace gases Research InfraStructure network) and GUAN (German Ultrafine Aerosol Network). Further details of the Melpitz station can be found in Poulain et al. (2011, 2014, 2020) and Van Pinxteren et al. (2024).

2.2 Single Particle Soot Photometer (SP2)

A single particle soot photometer (SP2) was used to investigate the physical properties of BC in this study. When a BC-containing particle passes through the laser beam of SP2, the BC core absorbs the laser light and emits an incandescence signal, with the peak intensity proportional to the BC mass (Schwarz et al., 2006). BC measured by this laser-induced incandescence (LII) method is referred to as refractory black carbon (rBC; Petzold et al., 2013). The mass equivalent diameter of rBC core was calculated assuming a density of 1.8 g m^{-3} (Bond and Bergstrom, 2007). The rBC detection size range of SP2 used in this study is 80-500nm in diameter.

As the rBC core is heated by the laser, its coating is thermally evaporated. The leading-edge-only (LEO) fitting method was applied to reconstruct the scattering signal associated with the coating (Gao et al., 2007). The overall rBC-containing particle's

https://doi.org/10.5194/egusphere-2026-5074
Preprint. Discussion started: 26 August 2026

diameter was determined from the LEO-fitted scattering signal using Mie theory (Bohren and Huffman, 1998), assuming a refractive index of 2.26 – 1.26i for the rBC core (Moteki et al., 2010) and 1.5 + 0i for the coating (Liu et al., 2014). Further information on the SP2 measurement principle is available elsewhere (Schwarz et al., 2008; Moteki and Kondo, 2010; Liu et al., 2014), while technical specifications for the TROPOS SP2 operated at Melpitz are provided in Yang et al. (2025).

The mixing state of rBC-containing particles was quantified using the mass ratio of non-BC coating to rBC core, expressed as both bulk population-averaged values (MR_{bulk}) and single-particle values (MR_i), following Liu et al. (2019):

$$MR_{bulk} = \frac{\rho_{coating}}{\rho_{rBC}} \times \left(\left(\frac{D_p}{D_c}\right)^3 - 1\right) \quad (1)$$

$$MR_i = \frac{\rho_{coating}}{\rho_{rBC}} \times \left(\left(\frac{D_{p,i}}{D_{c,i}}\right)^3 - 1\right) \quad (2)$$

Here, $\rho_{coating}$ is the density of non-BC coating, assumed to be 1.5 g m^{-3} (Zhao et al., 2021), and ρ_{rBC} is the density of rBC core, assumed to be 1.8 g cm^{-3} (Bond and Bergstrom, 2007). $D_{p,i}$ and $D_{c,i}$ represent the overall rBC-containing particle diameter and rBC core diameter for each individual particle, respectively. The ratio D_p/D_c indicates the bulk relative coating thickness and was calculated based on the total volume of coated particles and cores within a given time window (Liu et al., 2014) :

$$\frac{D_p}{D_c} = \sqrt[3]{\frac{\sum_i D_{p,i}^3}{\sum_i D_{c,i}^3}} \quad (3)$$

Due to the detection limit of the SP2 scattering detector, coating information cannot be retrieved for most of the particles with rBC cores smaller than ~160 nm. For cores larger than this threshold, coating data can be derived for over 80% of the rBC-containing particles, as shown in Fig. s1. Therefore, only rBC cores with diameters greater than 160 nm were included in the calculation of MR_{bulk}. In addition, the bulk D_p/D_c further reduces the influence of small-particle-related uncertainties, as their limited volume contributes negligibly to the total, thereby providing a more robust and representative estimate of the overall mixing state.

2.3 Multi-Angle Absorption Photometer (MAAP)

A Multi-Angle Absorption Photometer (MAAP, Thermo Fisher Scientific, MA, USA) was used to measure the aerosol absorption coefficient (b_{abs}) at 637 nm. To minimize the influence of light-scattering aerosol components on the angular distribution of backscattered light, measurements are conducted using three detectors positioned at different angles. The absorption coefficients are derived using a radiative transfer model that corrects for artefacts associated with filter-related light interactions. A detailed description of the instrument and its operating principles is provided by Petzold and Schönlinner (2004) and Petzold et al. (2005). In this study, a wavelength correction factor of 1.05 was applied to adjust the standard MAAP measurement wavelength from 660 nm to 637 nm, following Müller et al. (2011).

https://doi.org/10.5194/egusphere-2026-5074
Preprint. Discussion started: 26 August 2026

2.4 Black Carbon Absorption Properties

To investigate the lensing effect induced by non-BC coatings, the mass absorption cross-section (MAC) of BC serves as a key parameter for quantifying the enhancement of light absorption efficiency. MAC quantifies the light absorption efficiency per unit mass of BC, and an increase in MAC with the coating-to-core mass ratio is typically interpreted as evidence of absorption enhancement due to the lensing effect. MAC is defined as:

$$MAC = \frac{b_{abs}}{m_{rBC}} \quad (4)$$

where b_{abs} indicates the absorption coefficient and m_{rBC} indicates the mass concentration of rBC. In this study, b_{abs} and m_{rBC} were measured by MAAP and SP2, respectively.

In most studies, MAC is calculated using time-averaged values of b_{abs} and m_{rBC} over defined time intervals. However, at the Melpitz background station, hourly-resolved (1 hour) MAC estimates exhibited large uncertainty due to the frequently observed low rBC mass concentrations and small rBC sizes. Low rBC concentrations observed during the campaign (median: 0.23 μg m^{-3}) resulted in weak absorption signals, increasing the relative uncertainty in b_{abs} measurements by MAAP.(Petzold and Schönlinner, 2004). Additionally, the mass median diameter (MMD) of the rBC core size distribution at Melpitz was relatively small. The median MMD during the campaign was 179 nm, which is lower than the MMD exceeding 200 nm reported in many studies (Huang et al., 2012; Liu et al., 2014; Liu et al., 2019; Holanda et al., 2023). During summer, the average MMD was even smaller, around 150 nm. A smaller MMD implies a higher fraction of smaller rBC particles, which increases the uncertainty of SP2 measurements due to the instrument's limited detection efficiency for small cores (Schwarz et al., 2010). Although extrapolating a lognormal fit to the measured rBC mass size distribution can partially compensate for the detection limit (Kipling et al., 2013; Pileci et al., 2021), the low rBC concentrations at Melpitz reduce the statistical robustness of the size distribution. As a result, uncertainties in SP2 measurements persist.

Considering the combined uncertainties from both MAAP and SP2 measurements, the hourly-resolved calculated MAC values became increasingly unreliable as rBC concentrations decreased. In some cases, physically implausible MAC values exceeding 30 m^2 g^{-1} were observed. Moreover, as shown in Fig. s2, the hourly-resolved MAC didn't show a significant variation with the MR_{bulk}, due to the broad variability in MAC within each MR_{bulk} range, particularly at low MR_{bulk}. These limitations suggest that hourly-resolved MAC is not well-suited for investigating the lensing effect under the conditions encountered in this study.

Instead of calculating the hourly MAC value, the slope of a linear fit of b_{abs} as a function of m_{rBC} can be used to derive the MAC, consistent with its formal definition:

$$b_{abs} = MAC \times m_{rBC} \quad (5)$$

This linear fit method has been shown to provide more stable and representative MAC estimates by averaging out noise and minimizing the influence of individual low-signal data points (Schnaiter et al., 2019; Ohata et al., 2021; Savadkoohi et al., 2024). To investigate the lensing effect, we derived the MAC within different MR_{bulk} intervals to examine how MAC varies with coating. As suggested by Liu et al. (2015b), the standardized major axis (SMA) regression method was applied, as it takes into account uncertainties in both X and Y directions. SMA regression is particularly suitable when the two variables are

https://doi.org/10.5194/egusphere-2026-5074
Preprint. Discussion started: 26 August 2026

not measured on the same scale (Warton et al., 2006), which makes it appropriate for the b_{abs} versus m_{rBC} line-fitting in this study.

In addition, the theoretical MAC ($MAC_{Mie,i}$) and absorption enhancement ($E_{abs,i}$) were calculated for each individual rBC-containing particle to quantify the effect of coatings on particle-level light absorption:

$$MAC_{Mie,i} = \frac{C_{abs,i}^{coated}}{m_{rBC,i}} \quad (6)$$

$$E_{abs,i} = \frac{C_{abs,i}^{coated}}{C_{abs,i}^{core}} \quad (7)$$

$m_{rBC,i}$ is the mass of the rBC core in the *ith* individual rBC-containing particle measured by the SP2. $C_{abs,i}^{coated}$ and $C_{abs,i}^{core}$ denote the absorption cross-sections of the *ith* coated rBC-containing particle and of the same rBC core without its coating, respectively. These cross-sections were calculated at a wavelength of 637 nm using Mie theory, by assuming the coated rBC is a core-shell structure, with core size and coating thickness obtained from SP2 measurements. The refractive indices were assumed to be 1.95+0.96i (Moteki et al., 2023) for the rBC core and 1.53+0i for the coating(Ferrero et al., 2011). The Mie calculation was conducted using the open-source software PyMieScatt (Sumlin et al., 2018).

In addition, to provide a simplified assessment of how rBC mixing-state heterogeneity influences optical modeling, we compared measured MAC with MAC predicted by Mie-theory calculations. In many modeling studies, a single bulk (or average) coating value is applied to all rBC cores, assuming a homogeneous coating distribution and neglecting particle-to-particle mixing-state heterogeneity (e.g., Saliba et al., 2016; Liu et al., 2018; Zanatta et al., 2018). Under this homogeneous-mixing assumption, MAC was calculated from the SP2-measured rBC core size distribution as prescribed:

$$MAC_{Mie,homogeneous} = \frac{\sum_i n(D_{c,j}) \times C_{abs}(D_{p,j,})}{\sum_i m(D_{c,j})} \quad (8)$$

where $D_{c,j}$ is the midpoint diameter of the *jth* rBC core-size bin, $n(D_{c,j})$ and $m(D_{c,j})$ indicate the number and mass concentration from the *jth* bin of rBC core number and mass size distribution, respectively. $C_{abs}\ (D_{p,j})$ was the absorption cross section associated with the corresponding coated rBC diameter, $D_{p,j}$. Given a MR_{bulk}, the coated rBC diameter corresponding to $D_{p,j}$ can be derived:

$$D_{p,j} = D_{c,j} \times \sqrt[3]{1 + MR_{bulk} \times \frac{\rho_{rBC}}{\rho_{coating}}} \quad (9)$$

To account for mixing-state heterogeneity, we also calculated MAC at the single-particle level and then averaged across all rBC-containing particles:

$$MAC_{Mie,heterogeneous} = \frac{\sum_i MAC_{Mie,i}}{N} \quad (10)$$

Where the $MAC_{Mie,i}$ denotes the theoretical MAC of the *ith* individual rBC-containing particle, and N is the total number of rBC-containing particles included in the calculation. This approach incorporates coating information for individual rBC-containing particles and can, to some extent, account for the effect of particle-to-particle mixing-state heterogeneity on MAC. Although it does not fully capture the complexity of particle-to-particle variability, it provides a useful framework for comparing Mie-calculated MAC under different assumptions of mixing-state heterogeneity.

https://doi.org/10.5194/egusphere-2026-5074
Preprint. Discussion started: 26 August 2026

3. Results

3.1 Time series of rBC physical properties and temperature

Figure.1 shows the time series of rBC physical properties measured by SP2, absorption coefficient (b_{abs}) measured by MAAP, and ambient temperature. Measurements were conducted from August 2021 to February 2022, covering summer (August), autumn (October and November), and winter (December to February). September data are missing due to instrument maintenance. b_{abs} exhibited a similar variation in the mass concentration of rBC (m_{rBC}), representing the absorption of rBC.

In general, rBC properties varied with seasons. As shown in Fig. 2, m_{rBC} was significantly lower in summer, with the mean concentration of 0.16±0.12 μg m^{-3}, consistent with reduced emissions from biomass burning and coal combustion during the warm season (Yang et al., 2025; Atabakhsh et al., 2025). These very low concentrations increased the measurement uncertainties of both the SP2 and MAAP, as discussed in the methods.

The largest mass median diameter (MMD) was observed in winter, with a mean of 189±19 nm, while autumn exhibited a slightly smaller MMD of 182±20nm. The relatively large rBC sizes are attributed to solid fuel combustion, as rBC from biomass burning and coal combustion is generally larger than that from liquid fuel combustion, such as traffic emissions (Schwarz et al., 2008; Zhang et al., 2020). At Melpitz, enhanced solid-fuel contributions during cold periods, especially in winter (mean temperature of 3±4°C), have been linked to heating-related emissions, with more than 50% of the biomass-burning and coal-combustion influence transported from the east (Atabakhsh et al., 2023). In contrast, the much smaller MMD in summer, with a mean of 148 ± 24 nm, was associated with reduced biomass burning and coal combustion emissions, together with an enhanced influence of long-range transport (Atabakhsh et al., 2025; Yang et al., 2025), during which larger rBC particles are preferentially removed (Moteki et al., 2012; Che et al., 2022).

MR_{bulk} exhibited an opposite trend compared to m_{rBC} and MMD. The mean MR_{bulk} in summer (1.97±1.09) was higher than in autumn (1.22±0.65) and winter (1.41±1.08). The larger fraction of high MR_{bulk} values in summer (Fig. 2) may be related to a greater contribution from aged rBC from long transportation (Yang et al., 2025). In addition, the smaller MMD in this season indicates a higher proportion of small rBC cores, which tend to have thick coatings (Cheng et al., 2018). Autumn exhibited a relatively narrow MR_{bulk} (0.02 - 4.38) variation, and the median and mean MR_{bulk} during winter were similar to those in autumn, but the higher fraction of large MR_{bulk} may be associated with lower ambient temperature and higher residential heating emissions in the winter (Zhang et al., 2020; Yang et al., 2025).

https://doi.org/10.5194/egusphere-2026-5074
Preprint. Discussion started: 26 August 2026

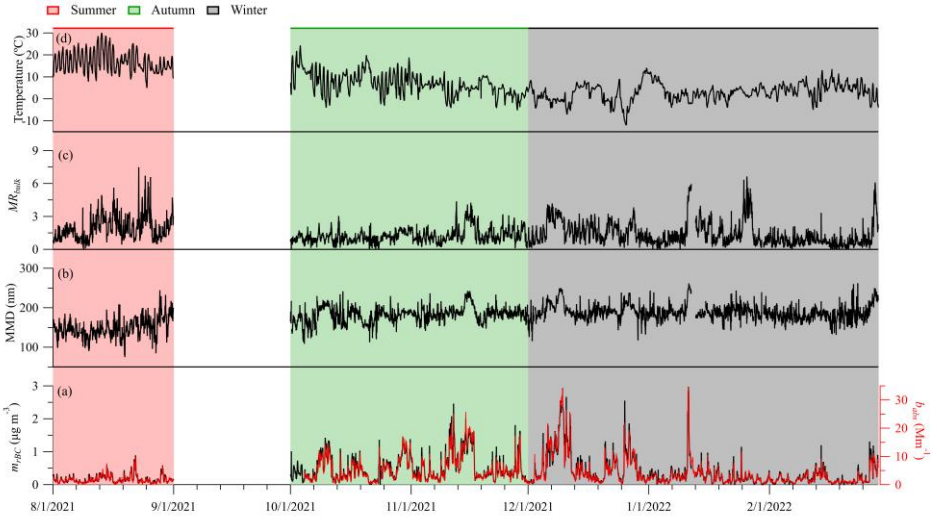

Figure 1: Time series of (a) mass concentration of rBC (m_{rBC}) and absorption coefficient (b_{abs}) (b) mass median diameter (MMD) (c) bulk mass ratio of coating to core (MR_{bulk}), and (d) temperature.

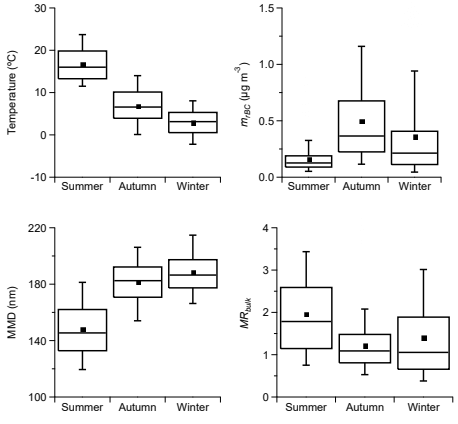

Figure 2: Statistical analysis of temperature and rBC properties for each season. The upper and lower edges of the box denote the 25% and 75% percentiles, respectively. The middle line and square markers indicate the median and average values, with whiskers indicating the 10% and 90% percentiles.

3.2 Absorption enhancement of BC-containing particles

To investigate the lensing effect, the MAC of rBC-containing particles was derived from standardized major axis (SMA) regression between b_{abs} and m_{rBC} across different MR_{bulk} intervals. The uncertainty of the SMA-derived MAC is represented by the confidence interval of the slope. These intervals were set at 0.5 increments, with the final bin containing all remaining data points. These intervals are from the $MR_{bulk} < 0.5$ to $MR_{bulk} > 3.5$. As shown in Fig. s3, the b_{abs} exhibited a strong correlation ($r^2 > 0.9$) for most intervals. In summer, the limited number of observations with $MR_{bulk} < 0.5$ was insufficient for reliable fitting; therefore, the first bin includes all data with $MR_{bulk} < 1$. Similarly, for autumn, the last bin contains all data with $MR_{bulk} > 3$.

https://doi.org/10.5194/egusphere-2026-5074
Preprint. Discussion started: 26 August 2026

In general, as shown in Fig. 3, MAC was observed to increase with MR_{bulk} in all seasons, though the dependence varied. In summer, MAC increased by 9 % for MR_{bulk} increase from 0 to 2, remained relatively stable (~11.50 m^2 g^{-1}) between MR_{bulk} of 2-3.5, and then increased significantly by 21% to 13.87 m^2 g^{-1} for MR_{bulk} > 3.5. Higher uncertainty in MAC estimation was also observed in this season, with one contributing factor being the extremely low concentration of rBC in summer. Although linear regression between absorption coefficient and rBC mass concentration was applied to reduce the influence of measurement uncertainty at very low concentrations, the persistently low concentrations in summer and the relatively narrow range of variation still increased the uncertainty of the fitted slope. This likely contributed substantially to the large uncertainty in the derived MAC.

In contrast, MAC in autumn and winter exhibited a more consistent increase with MR_{bulk}, accompanied by smaller uncertainty ranges. When MR_{bulk} increased from 0 to 2, MAC increased by 25 % in autumn and 20% in winter, respectively. At MR_{bulk} >2, the subsequent increases were more gradual, with MAC increasing by ~8% in both seasons. Across the same MR_{bulk} intervals, MAC values in autumn remained consistently higher than those in winter. One contributing factor to the observed uncertainties in MAC estimates and the differing dependence of MAC on MR_{bulk} is the heterogeneity in the mixing state of rBC-containing particles, which will be discussed in detail later.

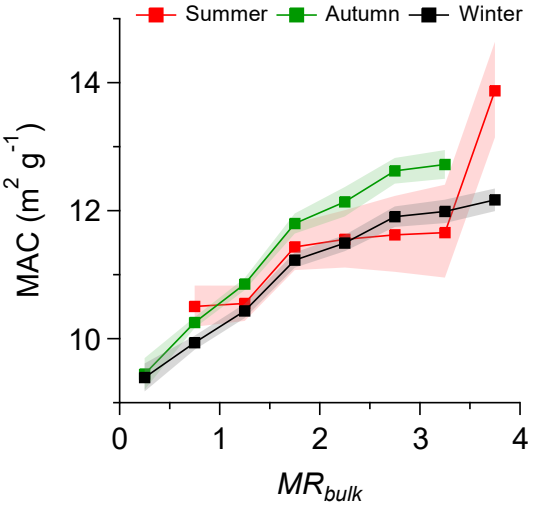

Figure 3: Variation of mass absorption cross-section (MAC) with bulk mass ratio of coating to core (MR_{bulk}) in different seasons. The shaded area represents the confidence interval of the SMA-fitted slope.

3.3 Mixing state heterogeneity of rBC-containing particles

Figure.4 shows that the coating-to-core mass ratio (MR_i) exhibits distinct distributions across different rBC core sizes, with the differences in mass contributions reflecting mixing state heterogeneity, indicating the coatings are not uniformly distributed across rBC cores. The rBC mass was selected to weight the MR distribution rather than the number because the mass plays a more important role in determining the optical properties of rBC-containing particles. Due to the detection limit of SP2, size-resolved MR_i data are only partially available for rBC cores smaller than 160 nm in diameter.

https://doi.org/10.5194/egusphere-2026-5074
Preprint. Discussion started: 26 August 2026

The mixing state heterogeneity exhibited evident seasonal differences. In summer, high rBC mass was only observed at MR_i < ~1.5, and the size-resolved MR_i showed an insignificant variation across MR_{bulk} intervals. As MR_{bulk} increased, rBC core mass in the high-MR_i region (MR_i > ~3) slightly increased. As shown in Fig.5 (a), the log-normal fitted mass size distribution (mSD) in summer was shifted to a smaller size compared to autumn and winter, with a higher fraction of rBC cores < 160 nm. Consequently, a substantial portion of the coating information is unavailable. The cumulative distribution function (CDF) of rBC mSD (Fig. 5(b)) indicates that 30–35 % of rBC mass fell below 160 nm, where the mixing state heterogeneity may differ from that of larger particles. This large fraction of missing mixing state information could contribute to the MR_{bulk} estimation, combined with the low mass concentration in summer, which further results in the uncertainties in MAC estimation shown in Fig. 3.

In contrast, autumn and winter exhibited a stronger dependence of mixing state heterogeneity on MR_{bulk}. As in summer, a persistent maximum in rBC mass in the regime where core diameters < 300 nm and MR_i < 1.5 was observed in both seasons. As MR_{bulk} increased, enhanced rBC mass appeared in the high-MR_i range (3 < MR_i < 20) with core diameters < 300nm. Under comparable MR_{bulk} intervals, rBC mass in the high-MR_i regime was more evident in autumn than in winter. In addition, for rBC >300nm, another relatively high rBC mass regime was also observed in the moderate MR_i range (2 < MR_i < 8) as the MR_{bulk} increased. Furthermore, the mSDs in these two seasons were shifted toward larger cores compared with summer (Fig. 5(a)), with only 10–25 % of rBC mass below 160 nm, which reduce the influence of missing mixing state information on the MR_{bulk} evaluation.

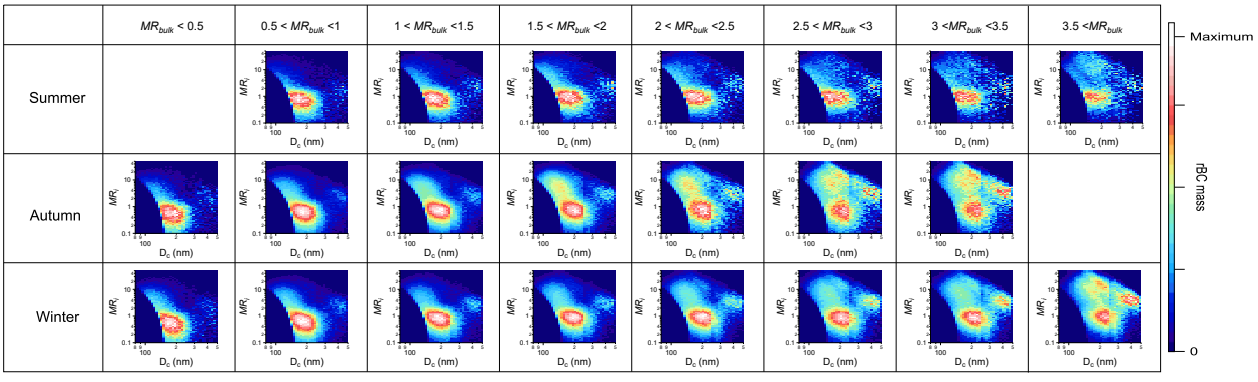

Figure 4: Size-resolved distributions of the particle-level coating-to-core mass ratio (MR_i). Columns denote the bulk mass ratio of coating to core (MR_{bulk}), and rows correspond to summer, autumn, and winter. In each panel, the x-axis shows the rBC core diameter (D_c) and the y-axis shows MR_i. Colors represent the rBC core mass, normalized to the maximum within each panel.

https://doi.org/10.5194/egusphere-2026-5074
Preprint. Discussion started: 26 August 2026

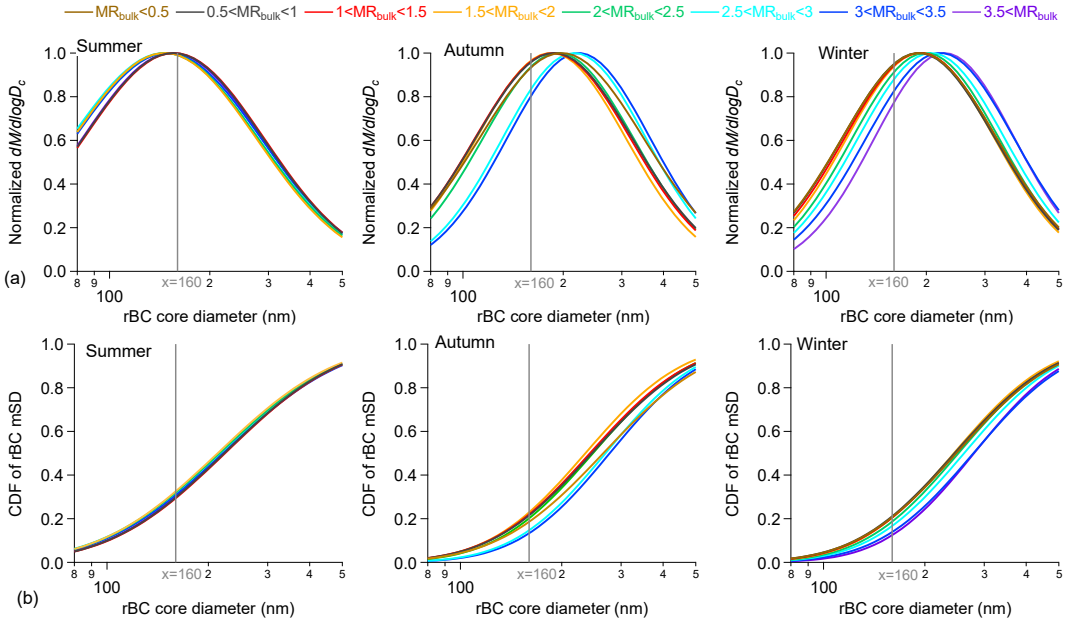

Figure 5: (a) Normalized log-normal fitted rBC core mass size distribution (mSD) and (b) cumulative distribution function (CDF) of mSD

3.4 Size-resolved E_{abs} and MAC for rBC-containing particles

Assuming the rBC-containing particle follows a spherical core-shell structure, the theoretical E_{abs} and MAC of measured single particles can be estimated by using Mie calculations. The SP2 detection limit prevents the determination of the mixing state for a subset of particles. To present the E_{abs} and MAC across the full MR_i and core-diameter range, we performed pure Mie calculations on a gridded MR–D_c domain, using the bin midpoints of MR_i and D_c as representative inputs for each grid cell (including regions where coating information is not retrievable). As shown in Fig. 6, the regions below the lower-left dashed boundary (D_c < ~140nm and MR_i<~10) and above the upper-right dashed boundary (D_c> ~250nm and MR_i > ~4) indicate the SP2 detection limits.

As shown in Fig.6 (a), E_{abs} did not constantly increase with MR_i. When MR_i <~1.5, E_{abs} below ~1.25 were observed for rBC cores between 80 and 500 nm, and for MR_i between ~1.5 and 6, E_{abs} was slightly higher (~2) for rBC cores > 200 nm than for smaller cores (~1.75). In contrast, when MR_i >6, E_{abs} exhibited higher values for cores < 200nm and reached up to a factor of 3 at MR_i > 20. However, as shown in Fig.4, such extremely thick coatings are rarely observed in the atmosphere and primarily represent a theoretical case. For most rBC-containing particles, the upper limit of E_{abs} is about 2, consistent with numerous field observations reporting values below 2 (Liu et al., 2017; Cappa et al., 2019; Yuan et al., 2021). Across the full MR_i range, only cores < 200 nm exhibited a monotonic increase in E_{abs}. For the cores > 200nm and MR_i > 1.5, E_{abs} exhibited a non-monotonic dependence on MR_i, with an initial maximum followed by a decline and a subsequent increase, likely due to the interference and scattering within the coating slightly reducing the light focusing on the BC core (Bond et al., 2006; Lack and Cappa, 2010). The mean $MAC_{Mie,i}$ exhibited a strong dependence on MR_i for rBC cores < 250 nm, showing an evident increase

https://doi.org/10.5194/egusphere-2026-5074
Preprint. Discussion started: 26 August 2026

with increasing MR_i (Fig. 6(b)). However, this dependence was less evident for larger cores. Additionally, when core diameter> 160 nm, $MAC_{Mie,i}$ generally decreased with increasing core size at a given MR_i. This is related to the relatively large size parameters approaching the geometric-optics regime, in which $MAC_{Mie,i}$ is inversely proportional to core diameter (Zanatta et al., 2018).

By comparing Fig.4 and Fig.6, the high-mass rBC was observed in the region with MR_i <2 and rBC core diameter < 300 nm in all panels of Fig.4, corresponding to the low E_{abs} and $MAC_{Mie,i}$ region in Fig.6. This suggests that, under ambient conditions, a substantial part of the rBC mass is associated with coatings that are not sufficiently thick to induce a strong lensing effect. As MR_{bulk} increased, a progressively larger fraction of rBC mass appeared in the high-E_{abs} and high-$MAC_{Mie,i}$ region. Although this increase involved only a relatively small fraction of the total rBC mass, MAC still increased (Fig.3). This suggests that the presence of even a limited amount of thickly coated rBC can increase the MAC of the overall particle population. In addition, in autumn and winter, an increase in rBC mass with core diameters > 300nm was also observed, corresponding to the moderate-E_{abs} and low-$MAC_{Mie,i}$ region in Fig.6, which may contribute to the weaker MAC enhancement when MR_{bulk} >2 in Fig.3.

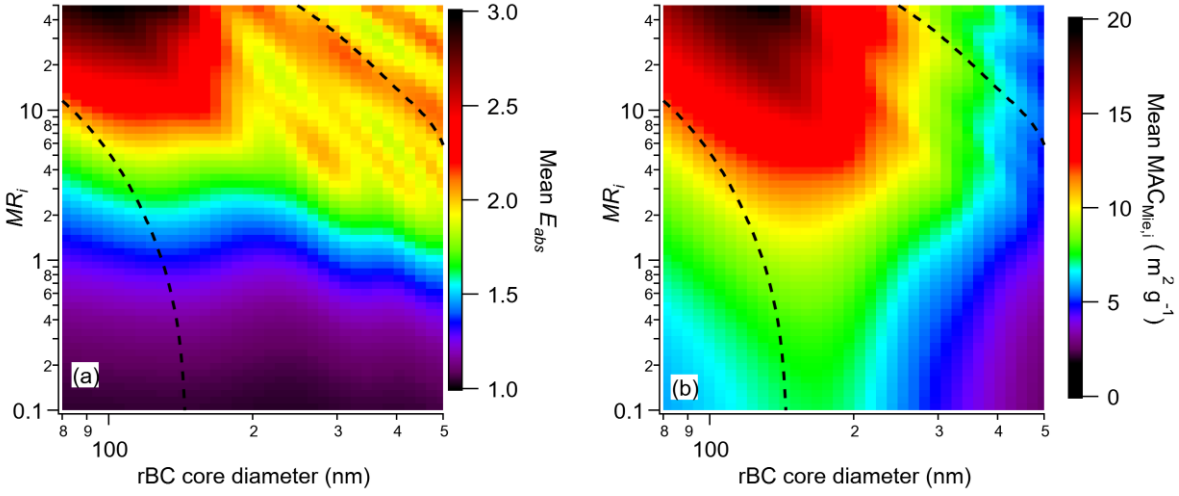

Figure 6: Two-dimensional distributions of (a) mean absorption enhancement (E_{abs}) and (b) mass absorption cross-section ($MAC_{Mie,i}$) from Mie calculations, mapped across coating-to-core mass ratio (MR_i)and rBC core diameter (D_c). The black dashed curves mark the SP2 coating-detection limits.

3.5 rBC mass distribution as a function of MR_i

To better quantify the influence of mixing state heterogeneity on the absorption abilities of coated rBC, the rBC mass distribution as a function of MR_i (MD_{MR}) was obtained from Fig.4 by integrating the rBC mass along the core size axis for each MR_i bin. As shown in Fig.7, differences in MD_{MR} are associated with variations in MAC across MR_{bulk} intervals. A similar result was reported in field measurements in Shanghai (Zhai et al., 2022), the unimodal structure represents a more homogeneous mixing state, while the bimodal structure indicates a more heterogeneous mixing state. In MD_{MR}, the first peak

https://doi.org/10.5194/egusphere-2026-5074
Preprint. Discussion started: 26 August 2026

at small MR_i (<3) was attributed to freshly emitted rBC, while the second peak at large MR_i (>3) was associated with the aged rBC. According to Liu et al. (2017), absorption enhancement induced by the coating was observed only at coating-to-core mass ratios> 3, with no enhancement for mass ratios < 1.5, and a transitional regime was defined between 1.5 and 3. Therefore, the shifts or the decrease in height of the first peak in MD_{MR} indicate a reduced fraction of rBC mass with little or no lensing effect, while the increase in the second peak height implies the enhanced fraction with significant lensing effect.

In summer, a more homogeneous mixing state was observed most of the time, as a unimodal MD_{MR}. When MR_{bulk}<1.5, MD_{MR} showed limited variation, with its peak remaining nearly unchanged, consistent with the nearly constant MAC. When MR_{bulk} increased to 2, the peak of MD_{MR} shifted slightly toward larger MR_i, and rBC mass modestly increased in the higher MR_i regime, leading to an increase in MAC from 10.55 m^2 g^{-1} to 11.43m^2 g^{-1}. Within the MR_{bulk} range of 1.5–3.5, MD_{MR} remained broadly similar, and MAC remained unchanged. At MR_{bulk} > 3.5, MAC increased sharply to 13.87 m^2 g^{-1}, coinciding with a pronounced increase in rBC mass at MR_i > 5.

Regarding autumn, continuous variation in MD_{MR} was observed with increasing MR_{bulk}. When MR_{bulk} <2, a more homogeneous mixing state was observed. As MR_{bulk} increased, the first peak of MD_{MR} shifted slightly to larger MR_i, while the height of the second peak gradually increased. During this stage, MAC values increased significantly, which is related to the increase in the fraction of thickly coated rBC. While for MR_{bulk}>2, a more heterogeneous mixing state was observed with bimodal MD_{MR}, and the second peak height remained nearly unchanged, whereas the height of the first peak decreased. This implies that the fraction of thickly coated rBC became higher compared to that of thinly coated rBC. In this phase, the enhancement of MAC was less significant compared to MR_{bulk} < 2.

In winter, MAC exhibited a pattern similar to that in autumn, with a strong increase from low to intermediate MR_{bulk}, followed by a weaker increase at higher MR_{bulk}. However, the corresponding variations in MD_{MR} differed from those in autumn. When MR_{bulk} <2, the more homogeneous mixing state was also observed; the shift of the first peak was more evident, whereas the enhancement of the second mode was less pronounced. At MR_{bulk} > 2, the second mode became more prominent, accompanied by a reduction in the first-mode peak. Across autumn and winter, larger MAC variability tended to occur under a more homogeneous mixing state (unimodal MD_{MR} or a weak second mode), whereas smaller MAC variability was associated with a more heterogeneous mixing state characterized by bimodal MD_{MR}. Similar results have been reported in previous studies(Fierce et al., 2016; Fierce et al., 2020b; Zhai et al., 2022). The different variation of MD_{MR} between autumn and winter may relate to different emission sources and atmospheric processes.

https://doi.org/10.5194/egusphere-2026-5074
Preprint. Discussion started: 26 August 2026

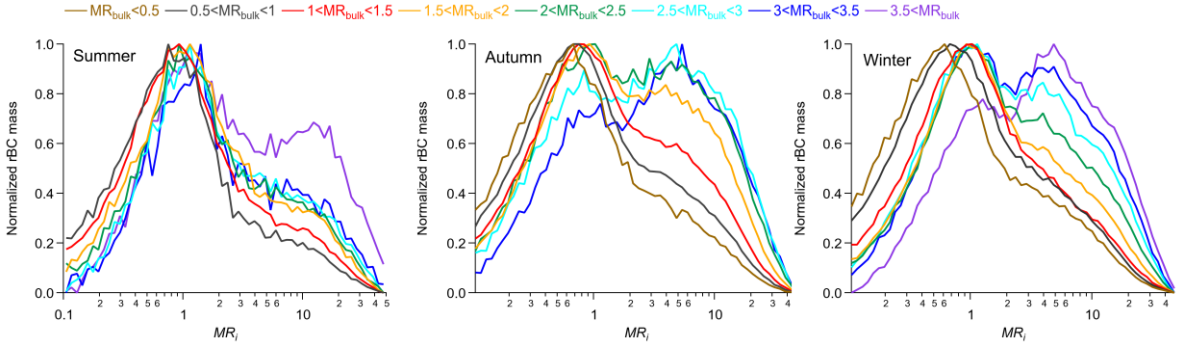

Figure 7: Normalized rBC mass distribution as a function of coating-to-core mass ratio (MR_i) for different seasons. The coloured lines represent normalized rBC mass, while the coloured square markers indicate the MAC values (from Fig. 3) corresponding to different bulk mass ratio of coating to core (MR_{bulk}) intervals.

Figure.8 further shows that, across all seasons, MAC increases as the rBC mass fraction at MR_i < 1.5 decreases from approximately 50 % to 30 %, while the fraction at MR_i >3 increases from approximately 10 % to 40 %. Some particles yielded negative coating thicknesses from the LEO fit. These non-physical values have been attributed to retrieval uncertainties in previous studies (Taylor et al., 2015; Krasowsky et al., 2018). In addition, the rBC mass fraction at MR_i <0 also decreases from approximately 50 % to 10 % with increasing overall coating level and MAC. This indicates a reduced contribution from thinly coated, or partially coated rBC particles, which exhibit little or no lensing enhancement. The concurrent decrease in mass fraction of negative coating therefore suggests that these non-physical values may be associated with such particles.

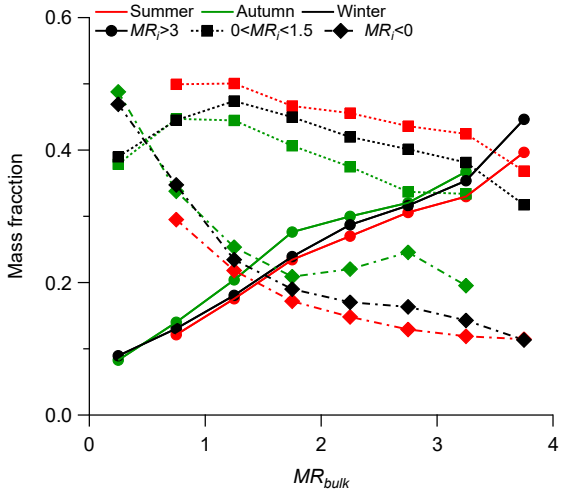

Figure 8: Variations of mass fractions of rBC in different coating-to-core mass ratio (MR_i) ranges with bulk mass ratio of coating to core (MR_{bulk}) for different seasons.

https://doi.org/10.5194/egusphere-2026-5074
Preprint. Discussion started: 26 August 2026

3.6 Seasonal comparison of mixing state heterogeneity

Seasonal comparison of MD_{MR} across different MR_{bulk} intervals was shown in Fig.9. For a given MR_{bulk} interval, distinct MD_{MR} were observed for different seasons. In summer, the normalized rBC mass at the high MR_i was consistently lower than the other two seasons, and the second peak only appeared when MR_{bulk} > 3.5. Nevertheless, the MAC of summer was not significantly lower than other seasons. This can be attributed to the larger fraction of rBC cores without coating information in summer (Fig. 5), particles below the SP2 detection limit are likely well aged and related to relatively high $MAC_{Mie,i}$ in Fig. 7. Such well-aged rBC likely originated from long-range transport and intense photochemical processing during summer (Yang et al., 2025). As for autumn and winter, the influence of rBC mass lacking coating information on MAC was less pronounced, as the majority of coating information was captured. Within the same MR_{bulk} interval, autumn exhibited a higher second peak height compared to winter, consistent with its higher MAC in autumn under comparable MR_{bulk} intervals.

As discussed above, with increasing MR_{bulk}, the increase in rBC mass occurred in different core-size regimes in autumn and winter. In autumn, the added rBC mass was more pronounced at core diameters < 300 nm (Fig. 4), whereas in winter it was more evident at core diameters > 300 nm. rBC from solid-fuel combustion is often associated with larger core sizes and thicker coatings (Schwarz et al., 2008; Liu et al., 2014; Zhang et al., 2020). Consistent with this, the larger MMDs observed in autumn and winter were linked to easterly winds (Fig. s4), which were also associated with higher mass concentrations, higher $MR_{bulk,}$ and lower temperature. Previous studies have similarly shown that easterly transport at Melpitz is mainly related to residential heating emissions from coal combustion and biomass-burning sources (Atabakhsh et al., 2023; 2025; Yang et al., 2025). In addition, the contribution of solid fuel emissions was higher in winter, where biomass burning organic aerosol (BBOA) and coal combustion organic aerosol (CCOA) together accounted for 38 % of total organic aerosol (OA), compared to only 13 % in autumn (Atabakhsh et al., 2025). In autumn and winter, as MR_{bulk} increased, easterly winds occurred more frequently than westerly winds (Fig. s5).

Together, these lines of evidence suggest a stronger influence of solid-fuel combustion under high MR_{bulk} conditions in autumn and winter. The particle-to-particle mixing-state distributions show that this high population-averaged aging level was partly attributed to the increased contribution from large-core rBC particles with relatively low absorption efficiency. This helps explain why MAC remained nearly unchanged once MR_{bulk} exceeded 2.5 in both seasons. Consequently, solid-fuel-influenced rBC populations exhibited lower MAC than populations with a similar bulk aging level but dominated by smaller, more efficiently absorbing cores.

https://doi.org/10.5194/egusphere-2026-5074
Preprint. Discussion started: 26 August 2026

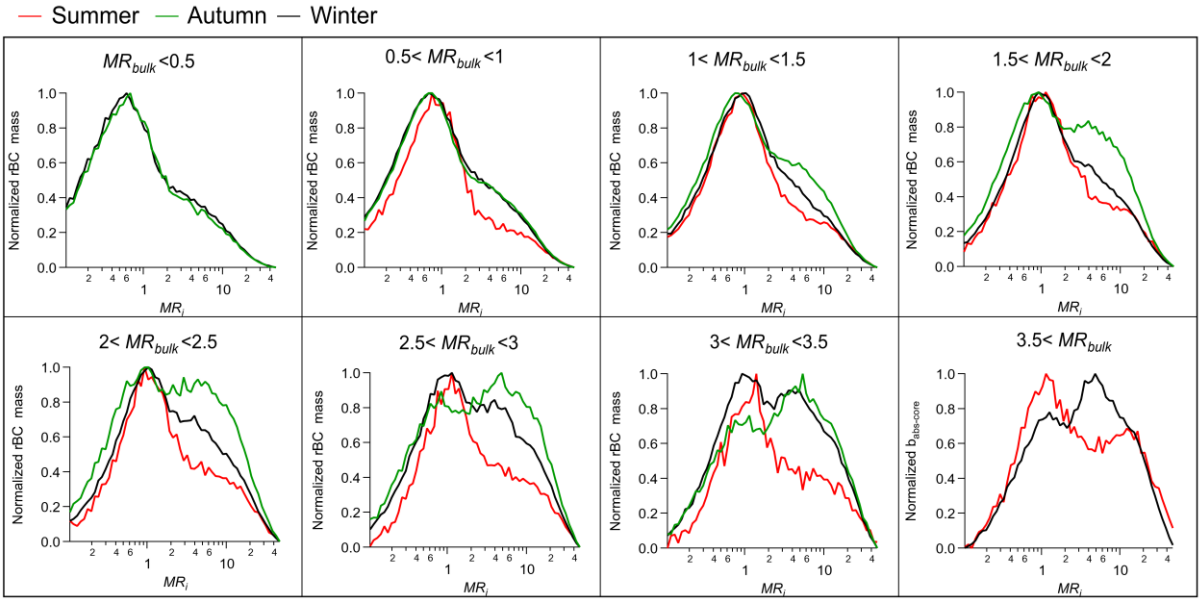

Figure 9: Seasonal comparison of normalized rBC mass distributions as a function of coating-to-core mass ratio (MR_i) ranges with bulk mass ratio of coating to core (MR_{bulk}).

3.7 Comparison between observations and Mie calculation

To assess how rBC mixing-state heterogeneity affects optical modelling, we compared MAC derived from measurements with MAC predicted by Mie calculations. The Mie-derived MACs of this chapter were calculated from the rBC sizes ranging from 80 nm to 500 nm, which is the detection limit of this SP2, and contains most of the rBC mass (Fig.5b). The measured MAC ($MAC_{measured}$) refers to the MAC values derived from the SMA fit between b_{abs} and m_{rBC} in Fig.3.

Following the approach described in Sect. 2.4, we calculated the $MAC_{Mie,\ homogeneous}$ for different MR_{bulk} intervals in each season, using the midpoint of each MR_{bulk} bin as input to the Mie model. As shown in Fig.10, $MAC_{Mie,homogeneous,}$ was consistently lower than the $MAC_{measured}$, with an average underestimation of 23%. The discrepancy was largest in autumn, ranging from 24 % to 33 %, compared with 12 %–29 % in summer and 19 %–32 % in winter. The homogeneous-mixing assumption partly contributes to this underestimation, which does not capture the preferential occurrence of thick coatings on smaller rBC cores. In addition, the MR_{bulk} was calculated only for rBC cores larger than 160 nm, which may contribute to the underestimation as well. As shown in Fig. s6, $MAC_{Mie,\ homogeneous}$ exhibited only limited seasonal variation. The variation in autumn and winter largely overlapped in autumn and winter because of their similar rBC core-size distributions.

In contrast, $MAC_{Mie,\ heterogeneous}$ was numerically closer to $MAC_{measured}$, with differences of less than 10 %. However, this numerical agreement does not necessarily indicate that $MAC_{Mie,\ heterogeneous}$ accurately reproduces the measured MAC. Particles outside the SP2 detection range were not included, which may bias the calculated values. In addition, the arithmetic averaging of single-particle MAC values may give disproportionate weight to the more numerous small-core rBC particles with thick coatings, even though their contribution to population-integrated absorption is relatively limited. Nevertheless, incorporating

https://doi.org/10.5194/egusphere-2026-5074
Preprint. Discussion started: 26 August 2026

single-particle formation partially captures mixing-state heterogeneity, as $MAC_{Mie,heterogeneous}$ better reproduces the variation pattern in $MAC_{measured}$, particularly a pronounced increase at lower MR_{bulk}, followed by a weaker increase at higher MR_{bulk} in autumn and winter.

The Mie-calculated MAC should therefore be interpreted qualitatively rather than as an exact quantitative reproduction of the measurements, since the absorption properties of rBC-containing particles in the atmosphere are influenced by multiple factors, including particle morphology, size, and the refractive indices of both the rBC core and the coating material(Bond et al., 2013; Romshoo et al., 2021; Chen et al., 2025). Nevertheless, under the same core–shell geometry and refractive-index assumptions, a simple assumption of mixing state heterogeneity leads to large discrepancies in MAC of the overall rBC population simulations. This comparison demonstrates that particle-to-particle mixing-state heterogeneity should be considered in parameterizations of BC absorption and estimates of its direct radiative effects. (Zhao et al., 2019; Zeng et al., 2024)

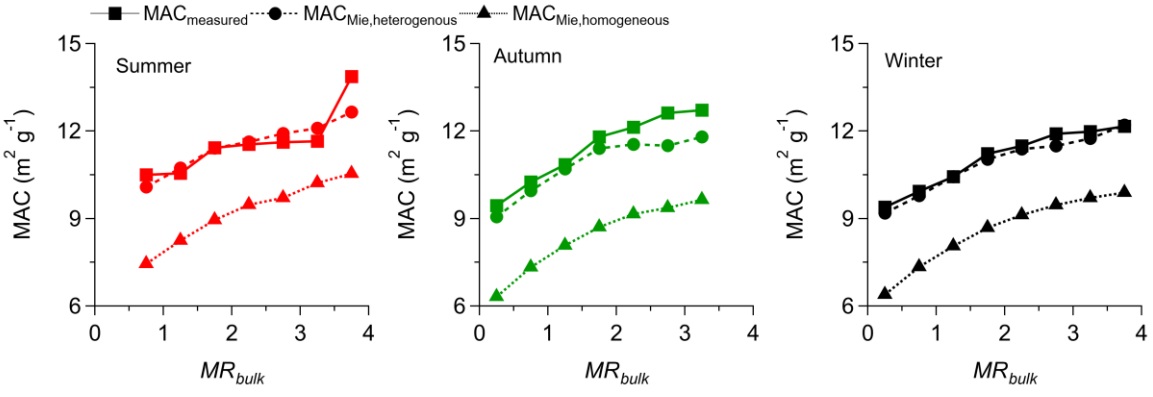

Figure 10: Comparison of MAC from Fig.3 ($MAC_{measured}$) and with Mie-calculated MAC for different seasons. Square markers denote the $MAC_{measured}$. Circle and triangle markers represent Mie-derived MAC based on the rBC core size distribution and single-particle information, referred to $MAC_{Mie,\ homogeneous}$ and $MAC_{Mie,\ heterogeneous}$, respectively.

4. Conclusion

Measurements of refractory black carbon (rBC) properties were conducted from August 2021 to February 2022 at the central European background site Melpitz, Germany. rBC properties were characterized for three seasons, with a particular focus on mass absorption cross-section (MAC) and mixing state. The mass ratio of coating to core was used to quantify the mixing state, both for the bulk rBC population (MR_{bulk}) and individual rBC particles (MR_i). The rBC mass distribution as a function of MR_i (MD_{MR}) was further used to characterize the mixing state heterogeneity

During summer, MAC showed only a weak dependence on MR_{bulk}, ranging from ~10.50 $m^2\ g^{-1}$ to 11.5 $m^2\ g^{-1}$. This observation coincides with a predominantly unchanged unimodal MD_{MR}, indicating a relatively homogeneous mixing state. In contrast, autumn and winter showed larger changes in mixing-state heterogeneity as MR_{bulk} increased, with MAC ranging from 9.44m^2 g^{-1} to 12.72 $m^2\ g^{-1}$ in the autumn and 9.39 $m^2\ g^{-1}$ to 12.17 $m^2\ g^{-1}$ in winter, respectively. In both seasons, the MD_{MR} evolved

https://doi.org/10.5194/egusphere-2026-5074
Preprint. Discussion started: 26 August 2026

from a unimodal to a bimodal distribution with increasing MR_{bulk}, indicating a more heterogeneous mixing state, and MAC enhancement was associated with shifts in the first mode at lower MR_i and an enhanced contribution of the second mode at higher MR_i. The sensitivity of MAC to changes in mixing state also depended on the initial degree of heterogeneity: changes within relatively homogeneous rBC populations were associated with stronger MAC variations, whereas further changes within already heterogeneous mixing states produced only limited MAC changes.

For a given MR_{bulk}, MAC was generally higher in the autumn compared with summer and winter, which was associated with a higher second mode of MD_{MR}, and a large contribution from thickly coated rBC particles. Furthermore, increases in rBC mass with core sizes > 300 nm were more frequently observed in autumn and winter. These large rBC cores, even with relatively thick coatings, tended to exhibit weaker absorption enhancement and thus lower MAC, consistent with increased contributions from biomass burning and coal combustion, particularly in winter.

Mie calculations further revealed substantial differences in the simulated MAC of the overall rBC population when particle-to-particle mixing-state heterogeneity was represented in different ways. When the mixing state of each individual particle was considered, the simulation better captured the variation in population-level MAC with MR_{bulk}, particularly in reproducing the pronounced MAC increase at lower MR_{bulk}, and the weaker increase at higher MR_{bulk}. Overall, these results highlight that an explicit representation of rBC mixing-state heterogeneity is essential for accurately simulating aerosol light absorption and for reducing uncertainties in estimates of rBC radiative forcing from regional to global scales.

Appendix A: Notation list

ACTRIS	Aerosols, Clouds, and Trace gases Research InfraStructure network
BBOA	biomass burning organic aerosol
BC	black carbon
b_{abs}	aerosol absorption coefficient
C_{abs}	absorption cross-section
CCOA	coal combustion organic aerosol
CDF	cumulative distribution function
D_c	refractory black carbon core diameter
D_p	overall diameter of an rBC-containing particle
D_p/D_c	bulk relative coating thickness
E_{abs}	absorption enhancement
$E_{abs,i}$	absorption enhancement of the ith individual rBC-containing particle
GUAN	German Ultrafine Aerosol Network

https://doi.org/10.5194/egusphere-2026-5074
Preprint. Discussion started: 26 August 2026

IPCC	Intergovernmental Panel on Climate Change
LEO	leading-edge-only fitting method
LII	laser-induced incandescence
MAAP	Multi-Angle Absorption Photometer
MAC	mass absorption cross-section
$MAC_{measured}$	measured mass absorption cross-section derived from SMA regression
$MAC_{Mie,i}$	Mie-calculated mass absorption cross-section of the *ith* individual rBC-containing particle
$MAC_{Mie,homogeneous}$	Mie-calculated mass absorption cross-section under the homogeneous-mixing assumption
$MAC_{Mie,heterogeneous}$	Mie-calculated mass absorption cross-section under the heterogeneous-mixing assumption
MD_{MR}	rBC mass distribution as a function of the single-particle coating-to-core mass ratio
MMD	mass median diameter
MR	mass ratio of non-BC coating to rBC core
MR_{bulk}	bulk population-averaged mass ratio of non-BC coating to rBC core
MR_i	single-particle mass ratio of non-BC coating to rBC core
m_{rBC}	mass concentration of refractory black carbon
mSD	rBC core mass size distribution
OA	organic aerosol
PM_{10}	particulate matter with an aerodynamic diameter of 10 micrometres or less
rBC	refractory black carbon
SMA	standardized major axis regression
SOA	secondary organic aerosol
SP2	Single Particle Soot Photometer
TEM	transmission electron microscopy
TROPOS	Leibniz Institute for Tropospheric Research

Author contributions. TM and YY designed the research. YY and JV collected the data at Melpitz. YY performed the data analysis. YY wrote the first draft of the manuscript. All co-authors contributed to the interpretation of the results as well as paper review and editing.

https://doi.org/10.5194/egusphere-2026-5074
Preprint. Discussion started: 26 August 2026

Data availability: Data are available upon request to the corresponding author.

Competing interests. The authors have no competing interests to declare.

Financial support. This research has been supported by the China Scholarship Council (grant no. 201908320539), ACTRIS2 (grant no. 654109).

References

Bohren, C. F. and Huffman, D. R.: Absorption and Scattering of Light by Small Particles, John Wiley & Sons, New York, NY, USA, 1998.

Adachi, K., Moteki, N., Kondo, Y., and Igarashi, Y.: Mixing states of light-absorbing particles measured using a transmission electron microscope and a single-particle soot photometer in Tokyo, Japan, Journal of Geophysical Research: Atmospheres, 121, 9153–9164, https://doi.org/10.1002/2016JD025153, 2016.

Atabakhsh, S., Poulain, L., Bigi, A., Coen, M. C., Pöhlker, M., and Herrmann, H.: Trends of PM1 aerosol chemical composition, carbonaceous aerosol, and source over the last 10 years at Melpitz (Germany), Atmospheric Environment, 346, 121075, https://doi.org/10.1016/j.atmosenv.2025.121075, 2025.

Atabakhsh, S., Poulain, L., Chen, G., Canonaco, F., Prévôt, A. S. H., Pöhlker, M., Wiedensohler, A., and Herrmann, H.: A 1-year aerosol chemical speciation monitor (ACSM) source analysis of organic aerosol particle contributions from anthropogenic sources after long-range transport at the TROPOS research station Melpitz, Atmos. Chem. Phys., 23, 6963–6988, 10.5194/acp-23-6963-2023, 2023.

Bond, T. C. and Bergstrom, R. W.: Light Absorption by Carbonaceous Particles: An Investigative Review, Aerosol Science and Technology, 40, 27–67, 10.1080/02786820500421521, 2007.

Bond, T. C., Habib, G., and Bergstrom, R. W.: Limitations in the enhancement of visible light absorption due to mixing state, Journal of Geophysical Research, 111, 10.1029/2006jd007315, 2006.

Bond, T. C., Doherty, S. J., Fahey, D. W., Forster, P. M., Berntsen, T., DeAngelo, B. J., Flanner, M. G., Ghan, S., Kärcher, B., Koch, D., Kinne, S., Kondo, Y., Quinn, P. K., Sarofim, M. C., Schultz, M. G., Schulz, M., Venkataraman, C., Zhang, H., Zhang, S., Bellouin, N., Guttikunda, S. K., Hopke, P. K., Jacobson, M. Z., Kaiser, J. W., Klimont, Z., Lohmann, U., Schwarz, J. P., Shindell, D., Storelvmo, T., Warren, S. G., and Zender, C. S.: Bounding the role of black carbon in the climate system: A scientific assessment, Journal of Geophysical Research: Atmospheres, 118, 5380–5552, 10.1002/jgrd.50171, 2013.

Cappa, C. D., Zhang, X., Russell, L. M., Collier, S., Lee, A. K. Y., Chen, C.-L., Betha, R., Chen, S., Liu, J., Price, D. J., Sanchez, K. J., McMeeking, G. R., Williams, L. R., Onasch, T. B., Worsnop, D. R., Abbatt, J., and Zhang, Q.: Light Absorption by Ambient Black and Brown Carbon and its Dependence on Black Carbon Coating State for Two California, USA, Cities in Winter and Summer, Journal of Geophysical Research: Atmospheres, 124, 1550–1577, 10.1029/2018jd029501, 2019.

Cappa, C. D., Onasch, T. B., Massoli, P., Worsnop, D. R., Bates, T. S., Cross, E. S., Davidovits, P., Hakala, J., Hayden, K. L., Jobson, B. T., Kolesar, K. R., Lack, D. A., Lerner, B. M., Li, S.-M., Mellon, D., Nuaaman, I., Olfert, J. S., Petäjä, T., Quinn, P. K., Song, C., Subramanian, R., Williams, E. J., and Zaveri, R. A.: Radiative Absorption Enhancements Due to the Mixing State of Atmospheric Black Carbon, Science, 337, 1078–1081, doi:10.1126/science.1223447, 2012.

Che, H., Segal-Rozenhaimer, M., Zhang, L., Dang, C., Zuidema, P., Dobracki, A., Sedlacek, A. J., Coe, H., Wu, H., Taylor, J., Zhang, X., Redemann, J., and Haywood, J.: Cloud processing and weeklong ageing affect biomass burning aerosol properties over the south-eastern Atlantic, Communications Earth & Environment, 3, 10.1038/s43247-022-00517-3, 2022.

https://doi.org/10.5194/egusphere-2026-5074
Preprint. Discussion started: 26 August 2026

Chen, B., Bai, Z., Cui, X., Chen, J., Andersson, A., and Gustafsson, Ö.: Light absorption enhancement of black carbon from urban haze in Northern China winter, Environmental Pollution, 221, 418–426, https://doi.org/10.1016/j.envpol.2016.12.004, 2017.

Chen, X., Ching, J., Wu, F., Matsui, H., Jacobson, M. Z., Zhang, F., Wang, Y., Zhang, Z., Liu, D., Zhu, S., Rudich, Y., Shi, Z., Yoo, H., Jeon, K.-J., and Li, W.: Locating the missing absorption enhancement due to multi–core black carbon aerosols, Nature Communications, 16, 10187, 10.1038/s41467-025-65079-2, 2025.

Cheng, Y., Li, S. M., Gordon, M., and Liu, P.: Size distribution and coating thickness of black carbon from the Canadian oil sands operations, Atmos. Chem. Phys., 18, 2653–2667, 10.5194/acp-18-2653-2018, 2018.

Feng, X., Wang, J., Teng, S., Xu, X., Zhu, B., Wang, J., Zhu, X., Yurkin, M. A., and Liu, C.: Can light absorption of black carbon still be enhanced by mixing with absorbing materials?, Atmospheric Environment, 253, 10.1016/j.atmosenv.2021.118358, 2021.

Ferrero, L., Mocnik, G., Ferrini, B. S., Perrone, M. G., Sangiorgi, G., and Bolzacchini, E.: Vertical profiles of aerosol absorption coefficient from micro-Aethalometer data and Mie calculation over Milan, Science of The Total Environment, 409, 2824–2837, https://doi.org/10.1016/j.scitotenv.2011.04.022, 2011.

Fierce, L., Bond, T. C., Bauer, S. E., Mena, F., and Riemer, N.: Black carbon absorption at the global scale is affected by particle-scale diversity in composition, Nat Commun, 7, 12361, 10.1038/ncomms12361, 2016.

Fierce, L., Onasch, T. B., Cappa, C. D., Mazzoleni, C., China, S., Bhandari, J., Davidovits, P., Fischer, D. A., Helgestad, T., Lambe, A. T., Sedlacek, A. J., 3rd, Smith, G. D., and Wolff, L.: Radiative absorption enhancements by black carbon controlled by particle-to-particle heterogeneity in composition, Proc Natl Acad Sci U S A, 117, 5196–5203, 10.1073/pnas.1919723117, 2020a.

Fierce, L., Onasch, T. B., Cappa, C. D., Mazzoleni, C., China, S., Bhandari, J., Davidovits, P., Fischer, D. A., Helgestad, T., Lambe, A. T., Sedlacek, A. J., Smith, G. D., and Wolff, L.: Radiative absorption enhancements by black carbon controlled by particle-to-particle heterogeneity in composition, Proceedings of the National Academy of Sciences, 117, 5196–5203, 10.1073/pnas.1919723117, 2020b.

Gao, R. S., Schwarz, J. P., Kelly, K. K., Fahey, D. W., Watts, L. A., Thompson, T. L., Spackman, J. R., Slowik, J. G., Cross, E. S., Han, J. H., Davidovits, P., Onasch, T. B., and Worsnop, D. R.: A Novel Method for Estimating Light-Scattering Properties of Soot Aerosols Using a Modified Single-Particle Soot Photometer, Aerosol Science and Technology, 41, 125–135, 10.1080/02786820601118398, 2007.

Healy, R. M., Wang, J. M., Jeong, C. H., Lee, A. K. Y., Willis, M. D., Jaroudi, E., Zimmerman, N., Hilker, N., Murphy, M., Eckhardt, S., Stohl, A., Abbatt, J. P. D., Wenger, J. C., and Evans, G. J.: Light-absorbing properties of ambient black carbon and brown carbon from fossil fuel and biomass burning sources, Journal of Geophysical Research: Atmospheres, 120, 6619–6633, 10.1002/2015jd023382, 2015.

Holanda, B. A., Franco, M. A., Walter, D., Artaxo, P., Carbone, S., Cheng, Y., Chowdhury, S., Ditas, F., Gysel-Beer, M., Klimach, T., Kremper, L. A., Krüger, O. O., Lavric, J. V., Lelieveld, J., Ma, C., Machado, L. A. T., Modini, R. L., Morais, F. G., Pozzer, A., Saturno, J., Su, H., Wendisch, M., Wolff, S., Pöhlker, M. L., Andreae, M. O., Pöschl, U., and Pöhlker, C.: African biomass burning affects aerosol cycling over the Amazon, Communications Earth & Environment, 4, 10.1038/s43247-023-00795-5, 2023.

Huang, X.-F., Sun, T.-L., Zeng, L.-W., Yu, G.-H., and Luan, S.-J.: Black carbon aerosol characterization in a coastal city in South China using a single particle soot photometer, Atmospheric Environment, 51, 21–28, 10.1016/j.atmosenv.2012.01.056, 2012.

Jacobson, M. Z.: Strong radiative heating due to the mixing state of black carbon in atmospheric aerosols, Nature, 409, 695–697, 10.1038/35055518, 2001.

Kipling, Z., Stier, P., Schwarz, J. P., Perring, A. E., Spackman, J. R., Mann, G. W., Johnson, C. E., and Telford, P. J.: Constraints on aerosol processes in climate models from vertically-resolved aircraft observations of black carbon, Atmospheric Chemistry and Physics, 13, 5969–5986, 10.5194/acp-13-5969-2013, 2013.

https://doi.org/10.5194/egusphere-2026-5074
Preprint. Discussion started: 26 August 2026

Krasowsky, T. S., McMeeking, G. R., Sioutas, C., and Ban-Weiss, G.: Characterizing the evolution of physical properties and mixing state of black carbon particles: from near a major highway to the broader urban plume in Los Angeles, Atmospheric Chemistry and Physics, 18, 11991–12010, 10.5194/acp-18-11991-2018, 2018.

Lack, D. A. and Cappa, C. D.: Impact of brown and clear carbon on light absorption enhancement, single scatter albedo and absorption wavelength dependence of black carbon, Atmos. Chem. Phys., 10, 4207–4220, 10.5194/acp-10-4207-2010, 2010.

Liu, C., Chung, C. E., Yin, Y., and Schnaiter, M.: The absorption Ångström exponent of black carbon: from numerical aspects, Atmospheric Chemistry and Physics, 18, 6259–6273, 10.5194/acp-18-6259-2018, 2018.

Liu, D., Taylor, J. W., Young, D. E., Flynn, M. J., Coe, H., and Allan, J. D.: The effect of complex black carbon microphysics on the determination of the optical properties of brown carbon, Geophysical Research Letters, 42, 613–619, 10.1002/2014gl062443, 2015a.

Liu, D., Allan, J. D., Young, D. E., Coe, H., Beddows, D., Fleming, Z. L., Flynn, M. J., Gallagher, M. W., Harrison, R. M., Lee, J., Prevot, A. S. H., Taylor, J. W., Yin, J., Williams, P. I., and Zotter, P.: Size distribution, mixing state and source apportionment of black carbon aerosol in London during wintertime, Atmospheric Chemistry and Physics, 14, 10061–10084, 10.5194/acp-14-10061-2014, 2014.

Liu, D., Joshi, R., Wang, J., Yu, C., Allan, J. D., Coe, H., Flynn, M. J., Xie, C., Lee, J., Squires, F., Kotthaus, S., Grimmond, S., Ge, X., Sun, Y., and Fu, P.: Contrasting physical properties of black carbon in urban Beijing between winter and summer, Atmospheric Chemistry and Physics, 19, 6749–6769, 10.5194/acp-19-6749-2019, 2019.

Liu, D., Whitehead, J., Alfarra, M. R., Reyes-Villegas, E., Spracklen, Dominick V., Reddington, Carly L., Kong, S., Williams, Paul I., Ting, Y.-C., Haslett, S., Taylor, Jonathan W., Flynn, Michael J., Morgan, William T., McFiggans, G., Coe, H., and Allan, James D.: Black-carbon absorption enhancement in the atmosphere determined by particle mixing state, Nature Geoscience, 10, 184–188, 10.1038/ngeo2901, 2017.

Liu, S., Aiken, A. C., Gorkowski, K., Dubey, M. K., Cappa, C. D., Williams, L. R., Herndon, S. C., Massoli, P., Fortner, E. C., Chhabra, P. S., Brooks, W. A., Onasch, T. B., Jayne, J. T., Worsnop, D. R., China, S., Sharma, N., Mazzoleni, C., Xu, L., Ng, N. L., Liu, D., Allan, J. D., Lee, J. D., Fleming, Z. L., Mohr, C., Zotter, P., Szidat, S., and Prevot, A. S. H.: Enhanced light absorption by mixed source black and brown carbon particles in UK winter, Nat Commun, 6, 8435, 10.1038/ncomms9435, 2015b.

Luo, J., Zhang, Y., Wang, F., and Zhang, Q.: Effects of brown coatings on the absorption enhancement of black carbon: a numerical investigation, Atmospheric Chemistry and Physics, 18, 16897–16914, 10.5194/acp-18-16897-2018, 2018.

Moteki, N., Kondo, Y., and Nakamura, S.-i.: Method to measure refractive indices of small nonspherical particles: Application to black carbon particles, Journal of Aerosol Science, 41, 513–521, 10.1016/j.jaerosci.2010.02.013, 2010.

Moteki, N., Ohata, S., Yoshida, A., and Adachi, K.: Constraining the complex refractive index of black carbon particles using the complex forward-scattering amplitude, Aerosol Science and Technology, 57, 678–699, 10.1080/02786826.2023.2202243, 2023.

Moteki, N., Kondo, Y., Oshima, N., Takegawa, N., Koike, M., Kita, K., Matsui, H., and Kajino, M.: Size dependence of wet removal of black carbon aerosols during transport from the boundary layer to the free troposphere, Geophysical Research Letters, 39, n/a–n/a, 10.1029/2012gl052034, 2012.

Müller, T., Henzing, J. S., de Leeuw, G., Wiedensohler, A., Alastuey, A., Angelov, H., Bizjak, M., Collaud Coen, M., Engström, J. E., Gruening, C., Hillamo, R., Hoffer, A., Imre, K., Ivanow, P., Jennings, G., Sun, J. Y., Kalivitis, N., Karlsson, H., Komppula, M., Laj, P., Li, S. M., Lunder, C., Marinoni, A., Martins dos Santos, S., Moerman, M., Nowak, A., Ogren, J. A., Petzold, A., Pichon, J. M., Rodriquez, S., Sharma, S., Sheridan, P. J., Teinilä, K., Tuch, T., Viana, M., Virkkula, A., Weingartner, E., Wilhelm, R., and Wang, Y. Q.: Characterization and intercomparison of aerosol absorption photometers: result of two intercomparison workshops, Atmospheric Measurement Techniques, 4, 245–268, 10.5194/amt-4-245-2011, 2011.

Ohata, S., Mori, T., Kondo, Y., Sharma, S., Hyvärinen, A., Andrews, E., Tunved, P., Asmi, E., Backman, J., Servomaa, H., Veber, D., Eleftheriadis, K., Vratolis, S., Krejci, R., Zieger, P., Koike, M., Kanaya, Y., Yoshida, A., Moteki, N., Zhao, Y.,

https://doi.org/10.5194/egusphere-2026-5074
Preprint. Discussion started: 26 August 2026

Tobo, Y., Matsushita, J., and Oshima, N.: Estimates of mass absorption cross sections of black carbon for filter-based absorption photometers in the Arctic, Atmos. Meas. Tech., 14, 6723–6748, 10.5194/amt-14-6723-2021, 2021.

Petzold, A. and Schönlinner, M.: Multi-angle absorption photometry—a new method for the measurement of aerosol light absorption and atmospheric black carbon, Journal of Aerosol Science, 35, 421–441, 10.1016/j.jaerosci.2003.09.005, 2004.

Petzold, A., Schloesser, H., Sheridan, P. J., Arnott, W. P., Ogren, J. A., and Virkkula, A.: Evaluation of Multiangle Absorption Photometry for Measuring Aerosol Light Absorption, Aerosol Science and Technology, 39, 40–51, 10.1080/027868290901945, 2005.

Petzold, A., Ogren, J. A., Fiebig, M., Laj, P., Li, S. M., Baltensperger, U., Holzer-Popp, T., Kinne, S., Pappalardo, G., Sugimoto, N., Wehrli, C., Wiedensohler, A., and Zhang, X. Y.: Recommendations for reporting "black carbon" measurements, Atmospheric Chemistry and Physics, 13, 8365–8379, 10.5194/acp-13-8365-2013, 2013.

Pileci, R. E., Modini, R. L., Bertò, M., Yuan, J., Corbin, J. C., Marinoni, A., Henzing, B., Moerman, M. M., Putaud, J. P., Spindler, G., Wehner, B., Müller, T., Tuch, T., Trentini, A., Zanatta, M., Baltensperger, U., and Gysel-Beer, M.: Comparison of co-located refractory black carbon (rBC) and elemental carbon (EC) mass concentration measurements during field campaigns at several European sites, Atmospheric Measurement Techniques, 14, 1379–1403, 10.5194/amt-14-1379-2021, 2021.

Poulain, L., Spindler, G., Birmili, W., Plass-Dülmer, C., Wiedensohler, A., and Herrmann, H.: Seasonal and diurnal variations of particulate nitrate and organic matter at the IfT research station Melpitz, Atmospheric Chemistry and Physics, 11, 12579–12599, 10.5194/acp-11-12579-2011, 2011.

Poulain, L., Birmili, W., Canonaco, F., Crippa, M., Wu, Z. J., Nordmann, S., Spindler, G., Prévôt, A. S. H., Wiedensohler, A., and Herrmann, H.: Chemical mass balance of 300 °C non-volatile particles at the tropospheric research site Melpitz, Germany, Atmospheric Chemistry and Physics, 14, 10145–10162, 10.5194/acp-14-10145-2014, 2014.

Poulain, L., Spindler, G., Grüner, A., Tuch, T., Stieger, B., van Pinxteren, D., Petit, J.-E., Favez, O., Herrmann, H., and Wiedensohler, A.: Multi-year ACSM measurements at the central European research station Melpitz (Germany) – Part 1: Instrument robustness, quality assurance, and impact of upper size cutoff diameter, Atmospheric Measurement Techniques, 13, 4973–4994, 10.5194/amt-13-4973-2020, 2020.

Romshoo, B., Müller, T., Pfeifer, S., Saturno, J., Nowak, A., Ciupek, K., Quincey, P., and Wiedensohler, A.: Optical properties of coated black carbon aggregates: numerical simulations, radiative forcing estimates, and size-resolved parameterization scheme, Atmospheric Chemistry and Physics, 21, 12989–13010, 10.5194/acp-21-12989-2021, 2021.

Romshoo, B., Müller, T., Ahlawat, A., Wiedensohler, A., Haneef, M. V., Imran, M., Warsi, A. B., Mandariya, A. K., Habib, G., and Pöhlker, M. L.: Significant contribution of fractal morphology to aerosol light absorption in polluted environments dominated by black carbon (BC), npj Climate and Atmospheric Science, 7, 10.1038/s41612-024-00634-0, 2024.

Saleh, R., Marks, M., Heo, J., Adams, P. J., Donahue, N. M., and Robinson, A. L.: Contribution of brown carbon and lensing to the direct radiative effect of carbonaceous aerosols from biomass and biofuel burning emissions, Journal of Geophysical Research: Atmospheres, 120, 10,285–210,296, https://doi.org/10.1002/2015JD023697, 2015.

Saliba, G., Subramanian, R., Saleh, R., Ahern, A. T., Lipsky, E. M., Tasoglou, A., Sullivan, R. C., Bhandari, J., Mazzoleni, C., and Robinson, A. L.: Optical properties of black carbon in cookstove emissions coated with secondary organic aerosols: Measurements and modeling, Aerosol Science and Technology, 50, 1264–1276, 10.1080/02786826.2016.1225947, 2016.

Savadkoohi, M., Pandolfi, M., Favez, O., Putaud, J.-P., Eleftheriadis, K., Fiebig, M., Hopke, P. K., Laj, P., Wiedensohler, A., Alados-Arboledas, L., Bastian, S., Chazeau, B., María, Á. C., Colombi, C., Costabile, F., Green, D. C., Hueglin, C., Liakakou, E., Luoma, K., Listrani, S., Mihalopoulos, N., Marchand, N., Močnik, G., Niemi, J. V., Ondráček, J., Petit, J.-E., Rattigan, O. V., Reche, C., Timonen, H., Titos, G., Tremper, A. H., Vratolis, S., Vodička, P., Funes, E. Y., Zíková, N., Harrison, R. M., Petäjä, T., Alastuey, A., and Querol, X.: Recommendations for reporting equivalent black carbon (eBC) mass concentrations based on long-term pan-European in-situ observations, Environment International, 185, 108553, https://doi.org/10.1016/j.envint.2024.108553, 2024.

https://doi.org/10.5194/egusphere-2026-5074
Preprint. Discussion started: 26 August 2026

Schnaiter, M.: Absorption amplification of black carbon internally mixed with secondary organic aerosol, Journal of Geophysical Research, 110, 10.1029/2005jd006046, 2005.

Schnaiter, M., Linke, C., Ibrahim, I., Kiselev, A., Waitz, F., Leisner, T., Norra, S., and Rehm, T.: Specifying the light-absorbing properties of aerosol particles in fresh snow samples, collected at the Environmental Research Station Schneefernerhaus (UFS), Zugspitze, Atmospheric Chemistry and Physics, 19, 10829–10844, 10.5194/acp-19-10829-2019, 2019.

Schwarz, J. P., Spackman, J. R., Gao, R. S., Perring, A. E., Cross, E., Onasch, T. B., Ahern, A., Wrobel, W., Davidovits, P., Olfert, J., Dubey, M. K., Mazzoleni, C., and Fahey, D. W.: The Detection Efficiency of the Single Particle Soot Photometer, Aerosol Science and Technology, 44, 612–628, 10.1080/02786826.2010.481298, 2010.

Schwarz, J. P., Gao, R. S., Spackman, J. R., Watts, L. A., Thomson, D. S., Fahey, D. W., Ryerson, T. B., Peischl, J., Holloway, J. S., Trainer, M., Frost, G. J., Baynard, T., Lack, D. A., de Gouw, J. A., Warneke, C., and Del Negro, L. A.: Measurement of the mixing state, mass, and optical size of individual black carbon particles in urban and biomass burning emissions, Geophysical Research Letters, 35, 10.1029/2008gl033968, 2008.

Schwarz, J. P., Gao, R. S., Fahey, D. W., Thomson, D. S., Watts, L. A., Wilson, J. C., Reeves, J. M., Darbeheshti, M., Baumgardner, D. G., Kok, G. L., Chung, S. H., Schulz, M., Hendricks, J., Lauer, A., Kärcher, B., Slowik, J. G., Rosenlof, K. H., Thompson, T. L., Langford, A. O., Loewenstein, M., and Aikin, K. C.: Single-particle measurements of midlatitude black carbon and light-scattering aerosols from the boundary layer to the lower stratosphere, Journal of Geophysical Research, 111, 10.1029/2006jd007076, 2006.

Sumlin, B. J., Heinson, W. R., and Chakrabarty, R. K.: Retrieving the aerosol complex refractive index using PyMieScatt: A Mie computational package with visualization capabilities, Journal of Quantitative Spectroscopy and Radiative Transfer, 205, 127–134, https://doi.org/10.1016/j.jqsrt.2017.10.012, 2018.

Taylor, J. W., Allan, J. D., Liu, D., Flynn, M., Weber, R., Zhang, X., Lefer, B. L., Grossberg, N., Flynn, J., and Coe, H.: Assessment of the sensitivity of core / shell parameters derived using the single-particle soot photometer to density and refractive index, Atmospheric Measurement Techniques, 8, 1701–1718, 10.5194/amt-8-1701-2015, 2015.

Tuch, T. M., Haudek, A., Müller, T., Nowak, A., Wex, H., and Wiedensohler, A.: Design and performance of an automatic regenerating adsorption aerosol dryer for continuous operation at monitoring sites, Atmos. Meas. Tech., 2, 417–422, 10.5194/amt-2-417-2009, 2009.

van Pinxteren, D., Engelhardt, V., Mothes, F., Poulain, L., Fomba, K. W., Spindler, G., Cuesta-Mosquera, A., Tuch, T., Muller, T., Wiedensohler, A., Loschau, G., Bastian, S., and Herrmann, H.: Residential Wood Combustion in Germany: A Twin-Site Study of Local Village Contributions to Particulate Pollutants and Their Potential Health Effects, ACS Environ Au, 4, 12–30, 10.1021/acsenvironau.3c00035, 2024.

Wang, J., Wang, J., Cai, R., Liu, C., Jiang, J., Nie, W., Wang, J., Moteki, N., Zaveri, R. A., Huang, X., Ma, N., Chen, G., Wang, Z., Jin, Y., Cai, J., Zhang, Y., Chi, X., Holanda, B. A., Xing, J., Liu, T., Qi, X., Wang, Q., Pohlker, C., Su, H., Cheng, Y., Wang, S., Hao, J., Andreae, M. O., and Ding, A.: Unified theoretical framework for black carbon mixing state allows greater accuracy of climate effect estimation, Nat Commun, 14, 2703, 10.1038/s41467-023-38330-x, 2023.

Wang, Q., Cao, J., Han, Y., Tian, J., Zhu, C., Zhang, Y., Zhang, N., Shen, Z., Ni, H., Zhao, S., and Wu, J.: Sources and physicochemical characteristics of black carbon aerosol from the southeastern Tibetan Plateau: internal mixing enhances light absorption, Atmospheric Chemistry and Physics, 18, 4639–4656, 10.5194/acp-18-4639-2018, 2018.

Wang, Y., Liu, F., He, C., Bi, L., Cheng, T., Wang, Z., Zhang, H., Zhang, X., Shi, Z., and Li, W.: Fractal Dimensions and Mixing Structures of Soot Particles during Atmospheric Processing, Environmental Science & Technology Letters, 4, 487–493, 10.1021/acs.estlett.7b00418, 2017.

Wang, Y., Li, W., Huang, J., Liu, L., Pang, Y., He, C., Liu, F., Liu, D., Bi, L., Zhang, X., and Shi, Z.: Nonlinear Enhancement of Radiative Absorption by Black Carbon in Response to Particle Mixing Structure, Geophysical Research Letters, 48, 10.1029/2021gl096437, 2021.

Warton, D. I., Wright, I. J., Falster, D. S., and Westoby, M.: Bivariate line-fitting methods for allometry, Biological Reviews, 81, 259–291, https://doi.org/10.1017/S1464793106007007, 2006.

https://doi.org/10.5194/egusphere-2026-5074
Preprint. Discussion started: 26 August 2026

Wu, C., Wu, D., and Yu, J. Z.: Quantifying black carbon light absorption enhancement with a novel statistical approach, Atmospheric Chemistry and Physics, 18, 289–309, 10.5194/acp-18-289-2018, 2018.

Xie, C., Xu, W., Wang, J., Liu, D., Ge, X., Zhang, Q., Wang, Q., Du, W., Zhao, J., Zhou, W., Li, J., Fu, P., Wang, Z., Worsnop, D., and Sun, Y.: Light absorption enhancement of black carbon in urban Beijing in summer, Atmospheric Environment, 213, 499–504, https://doi.org/10.1016/j.atmosenv.2019.06.041, 2019.

Yang, Y., Müller, T., Poulain, L., Atabakhsh, S., Holanda, B. A., Voigtländer, J., Arora, S., and Pöhlker, M. L.: Microphysical properties of refractory black carbon aerosols for different air masses at a central European background site, Atmos. Chem. Phys., 25, 8637–8655, 10.5194/acp-25-8637-2025, 2025.

Yuan, J., Modini, R. L., Zanatta, M., Herber, A. B., Müller, T., Wehner, B., Poulain, L., Tuch, T., Baltensperger, U., and Gysel-Beer, M.: Variability in the mass absorption cross section of black carbon (BC) aerosols is driven by BC internal mixing state at a central European background site (Melpitz, Germany) in winter, Atmospheric Chemistry and Physics, 21, 635–655, 10.5194/acp-21-635-2021, 2021.

Yus-Díez, J., Via, M., Alastuey, A., Karanasiou, A., Minguillón, M. C., Perez, N., Querol, X., Reche, C., Ivančič, M., Rigler, M., and Pandolfi, M.: Absorption enhancement of black carbon particles in a Mediterranean city and countryside: effect of particulate matter chemistry, ageing and trend analysis, Atmos. Chem. Phys., 22, 8439–8456, 10.5194/acp-22-8439-2022, 2022.

Zanatta, M., Laj, P., Gysel, M., Baltensperger, U., Vratolis, S., Eleftheriadis, K., Kondo, Y., Dubuisson, P., Winiarek, V., Kazadzis, S., Tunved, P., and Jacobi, H.-W.: Effects of mixing state on optical and radiative properties of black carbon in the European Arctic, Atmospheric Chemistry and Physics, 18, 14037–14057, 10.5194/acp-18-14037-2018, 2018.

Zeng, L., Tan, T., Zhao, G., Du, Z., Hu, S., Shang, D., and Hu, M.: Overestimation of black carbon light absorption due to mixing state heterogeneity, npj Climate and Atmospheric Science, 7, 10.1038/s41612-023-00535-8, 2024.

Zhai, J., Yang, X., Li, L., Bai, B., Liu, P., Huang, Y., Fu, T. M., Zhu, L., Zeng, Z., Tao, S., Lu, X., Ye, X., Wang, X., Wang, L., and Chen, J.: Absorption Enhancement of Black Carbon Aerosols Constrained by Mixing-State Heterogeneity, Environ Sci Technol, 56, 1586–1593, 10.1021/acs.est.1c06180, 2022.

Zhang, Y., Zhang, Q., Yao, Z., and Li, H.: Particle Size and Mixing State of Freshly Emitted Black Carbon from Different Combustion Sources in China, Environ Sci Technol, 54, 7766–7774, 10.1021/acs.est.9b07373, 2020.

Zhang, Y., Favez, O., Canonaco, F., Liu, D., Močnik, G., Amodeo, T., Sciare, J., Prévôt, A. S. H., Gros, V., and Albinet, A.: Evidence of major secondary organic aerosol contribution to lensing effect black carbon absorption enhancement, npj Climate and Atmospheric Science, 1, 10.1038/s41612-018-0056-2, 2018.

Zhao, G., Zhao, W., and Zhao, C.: Method to measure the size-resolved real part of aerosol refractive index using differential mobility analyzer in tandem with single-particle soot photometer, Atmospheric Measurement Techniques, 12, 3541–3550, 10.5194/amt-12-3541-2019, 2019.

Zhao, G., Tan, T., Zhu, Y., Hu, M., and Zhao, C.: Method to quantify black carbon aerosol light absorption enhancement with a mixing state index, Atmos. Chem. Phys., 21, 18055–18063, 10.5194/acp-21-18055-2021, 2021.